

Viscoelastic Characterization of Phantoms for Ultrasound Elastography Created Using Low- and High-Viscosity Poly(vinyl alcohol) with Ethylene Glycol as the Cryoprotectant

Sapna R. Bisht, Bhanu Prasad Marri, Jayashree Karmakar, and Karla P. Mercado Shekhar*



Cite This: *ACS Omega* 2024, 9, 8352–8361



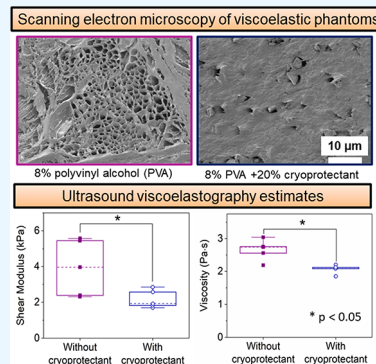
Read Online

ACCESS |

Metrics & More

Article Recommendations

ABSTRACT: Ultrasound elastography enables noninvasive characterization of the tissue mechanical properties. Phantoms are widely used in ultrasound elastography for developing, testing, and validating imaging techniques. Creating phantoms with a range of viscoelastic properties relevant to human organs and pathological conditions remains an active area of research. Poly(vinyl alcohol) (PVA) cryogel phantoms offer a long shelf life, robustness, and convenient handling and storage. The goal of this study was to develop tunable phantoms using PVA with a clinically relevant range of viscoelastic properties. We combined low- and high-viscosity PVA to tune the viscoelastic properties of the phantom. Further, phantoms were created with an ethylene glycol-based cryoprotectant to determine whether it reduces the variability in the viscoelastic properties. Scanning electron microscopy (SEM) was performed to evaluate the differences in microstructure between phantoms. The density, longitudinal sound speed, and acoustic attenuation spectra (5–20 MHz) of the phantoms were measured. The phantoms were characterized using a shear wave viscoelastography approach assuming the Kelvin–Voigt model. Microstructural differences were revealed by SEM between phantoms with and without a cryoprotectant and with different PVA mixtures. The longitudinal sound speed and attenuation power-law fit exponent of the phantoms were within the clinical range (1510–1571 m/s and 1.23–1.38, respectively). The measured shear modulus (G) ranged from 3.3 to 17.7 kPa, and the viscosity (η) ranged from 2.6 to 7.3 Pa·s. The phantoms with the cryoprotectant were more homogeneous and had lower shear modulus and viscosity ($G = 2.17 \pm 0.2$ kPa; $\eta = 2.0 \pm 0.05$ Pa·s) than those without a cryoprotectant ($G = 3.93 \pm 0.7$ kPa; $\eta = 2.6 \pm 0.14$ Pa·s). Notably, phantoms with relatively constant viscosities and varying shear moduli were achieved by this method. These findings advance the development of well-characterized viscoelastic phantoms for use in elastography.



INTRODUCTION

Ultrasound shear wave elastography is a widely reported technique for the noninvasive characterization of tissue mechanical properties. The accuracy and reliability of ultrasound elastography depend considerably on the availability of realistic tissue-mimicking phantoms that closely mimic the viscoelastic behavior of biological tissues. Tissue-mimicking phantoms play an important role in developing and validating new algorithms. Phantoms also play a role in training novice sonographers in new imaging techniques. It has been shown that assuming viscoelastic tissues to be elastic can produce large errors in imaging estimates.^{1,2} Therefore, ultrasound system manufacturers have started incorporating viscoelasticity imaging or viscoelastography into their devices to enable accurate assessment of inherently viscoelastic tissues.^{3,4} Despite these advancements, there is a need to develop standardized protocols and properly characterize phantoms with a clinically relevant range of viscoelastic properties, mimicking healthy and diseased tissues. The Quantitative Imaging Biomarker Alliance (QIBA) has emphasized the role

of phantoms in validating novel techniques and algorithms, including viscoelastography.⁵ Although elastic phantoms are commercially available for conventional B-Mode imaging, Doppler imaging, and elastography, standard viscoelastic phantoms are not widely available.

Phantoms fabricated with agar, gelatin, mixtures of gelatin and oil, and copolymers in mineral oil or silicone have been reported for applications in ultrasound elastography that incorporate viscous behavior.^{6–11} Poly(vinyl alcohol) (PVA) is a polymer that has mostly been reported for elastography using elastic material assumptions.^{12,13} PVA hydrogels have several advantages, such as easy fabrication, flexibility, toughness, long shelf life, and reproducibility.¹⁴ The range of

Received: November 19, 2023

Revised: January 15, 2024

Accepted: January 31, 2024

Published: February 9, 2024



Table 1. Characteristics of Different PVA Polymers Used in This Study

sample code (PVA _{viscosity} -%hydrolysis)	viscosity (mPa·s) (at 4% aq. H ₂ O, 20 °C)	average molecular weight (g/mol)	degree of hydrolysis (%)	product details (ID and supplier details)
PVA _{2.5cP-80%}	2.5–3.5	6,000	80	22225 - Polysciences, Inc., 400 Valley Road, Warrington, PA, USA.
PVA _{45cP-88%}	45–55	125,000	88	04398 - Polysciences, Inc., 400 Valley Road, Warrington, PA, USA.
PVA _{3.5cP-98%}	3.5–4.5	13,000–23,000	98–98.8	348406 - Sigma-Aldrich, 3050 Spruce Street, Saint Louis, MO, USA.
PVA _{27cP-99.5%}	27–33	Not available	99.5	Elvanol 71–30, Kuraray America, Inc., Houston, USA.

Table 2. Compositions of Phantoms Fabricated with a Cryoprotectant Liquid and PVA of Different Viscosities and Percent Degrees of Hydrolysis

total % concentration of PVA	PVA _{2.5cP-80%}	PVA _{45cP-88%}	PVA _{27 cP-99.5%}	PVA _{3.5 cP-99%}	status of gel formation
15	10	5			not formed
10		10			not formed
5		5			not formed
15		5	10		formed
15	5		10		formed
10			10		formed
10	10				not formed
10	5		5		formed
7.5	2.5		5		formed
5			5		formed
10			5	5	formed
11			6	5	formed
13			8	5	formed
15			10	5	formed

Young's modulus and viscosity of PVA phantoms reported in the literature are 1.6–615 kPa and 1.63–17.7 Pa·s, respectively, depending upon the number of freeze–thaw (FT) cycles, PVA concentration, and measurement method.^{8,15,16} Our group recently reported the viscoelastic nature of PVA and the feasibility to add glycerol to modify its properties.¹⁵ However, developing tunable phantoms using PVA with a clinically relevant range of viscoelastic properties remains an active area of research. The ability to create well-characterized PVA phantoms with a wide range of viscoelastic properties can aid in developing accurate viscoelastography techniques and improving diagnostic outcomes.

In addition, a few study protocols added a cryoprotectant liquid to PVA phantoms.^{12,17} The cryoprotectant liquid was used to reduce the formation of ice crystals during the FT cycle, which may damage the polymer cross-links, by lowering the freezing point. However, the effect of the cryoprotectant on the acoustic and mechanical properties of phantoms has not been systematically characterized.

The aim of the present work was to fabricate tissue-mimicking phantoms using different concentrations of varying viscosities of PVA to achieve a broad range of viscoelastic phantoms. We also evaluated the effect of adding an ethylene glycol-based cryoprotectant liquid on shear wave viscoelastography measurements. The density, longitudinal sound speed, and acoustic attenuation of the phantoms were measured. The phantom microstructure was also visualized by using scanning electron microscopy (SEM).

METHODS

Cryoprotectant-Based PVA Phantom Fabrication

Procedure. To assess the effect of the cryoprotectant on the acoustic and mechanical properties of the phantoms,

samples without the cryoprotectant were fabricated, comprising 8% w/v PVA (Elvanol 71–30, Kuraray America, Inc., Houston, USA), silicon carbide (SiC) acoustic scatterers (2% w/v, 600 mesh, Sarrah, India), and 90% v/v degassed, deionized water.^{12,15} Samples with the cryoprotectant were made with the same concentration of PVA and SiC, except with 70% v/v degassed, deionized water and 20% v/v ethylene glycol-based cryoprotectant liquid (antifreeze coolant, Waxpol Industries Ltd., Ranchi, India).

A mixture of cryoprotectant liquid and degassed, deionized water was first heated for 300 s using a 700-W microwave (NN-ST266B FDG, Panasonic, India) to attain a temperature of 80 °C. To degas the solution, the mixture was placed under vacuum at –700 mmHg for 10 min. PVA powder and silicon carbide particles were slowly added into the mixture with continuous stirring to avoid lumps or bubble formation. The solution was microwaved again for 300 s until the temperature reached 90 °C, ensuring the PVA powder dissolved completely. The solution was placed onto a thermal stir plate with a magnetic bar rotating at 500 rpm for 15 min to achieve a homogeneous solution. Then, the solution was degassed under vacuum at –700 mmHg for 30 min. The beaker was then covered with a plastic wrap and placed on a lab bench undisturbed for 30 min to bring the solution to room temperature. A thin layer of air bubbles, which formed at the top of the liquid surface, was carefully removed. The PVA solution was poured into phantom molds and covered with plastic wrap. The PVA solution was poured in molds to form cubic phantoms (25 mm per side) and cylindrical phantoms (75 mm diameter and 25 mm height). The cubic phantoms were used to measure their density, longitudinal sound speed, and acoustic attenuation. The cylindrical phantoms were characterized by ultrasound shear wave elastography. The

phantoms were subjected to a 24 h FT cycle, which included 0.5 h at 4 °C, 17.5 h of freezing at −20 °C, and 4 h of thawing at 4 °C. The samples were then placed on the lab bench at room temperature for 2 h. After the completion of 24 h, samples fabricated with the cryoprotectant were stored in distilled water with a 20% v/v cryoprotectant liquid to prevent the cryoprotectant from leaching out of the phantom. Samples made without the cryoprotectant were stored in only distilled water. Five independent samples per phantom type were prepared.

Phantom Preparation with a Combination of High- and Low-Molecular Weight PVA. Stock PVA powders with different viscosities and percentages of hydrolysis are commercially available. PVA powders with four different viscosities (2.5, 3.5, 27, and 45 mPa·s) and four different percent degrees of hydrolysis (80, 88, 98, and 99.5%) were used. The characteristics of the different PVA are reported in Table 1. The phantom compositions included PVA (10–15% w/v) with two different viscosities and/or two different percent degrees of hydrolysis, SiC particles, degassed deionized water (64–69% w/v), and cryoprotectant liquid (20% v/v). The procedure outlined in the previous section was followed to prepare the samples with different concentrations of low-viscosity and high-viscosity PVA. Five independent samples per phantom type were prepared per group.

The compositions of phantoms made with combinations of PVA with different viscosities and varying degrees of hydrolysis are shown in Table 2. PVA with ≥98% hydrolysis, i.e., PVA_{3.5cP-98%} and PVA_{27cP-99.5%}, were able to form gel phantoms and were stable. However, PVA with 80 and 88% hydrolysis, i.e., PVA_{2.5cP-80%} and PVA_{45cP-88%}, could not form stable gel phantoms. The inability to gel completely may be because PVA did not dissolve properly in the solution, and hence, PVA clumps were formed. For the PVA with 45 cP viscosity, the phantom solution was too viscous and did not freeze well during the FT cycle. Even as the number of FT cycles were increased to three, the phantom solution did not form into gel and remained a highly viscous fluid. Thus, subsequent phantoms were fabricated using the two PVA types with at least 98% hydrolysis, i.e., PVA_{3.5cP-98%} and PVA_{27cP-99.5%}. Four combinations of different concentrations of PVA_{27cP-99.5%}, ranging from 5 to 10% w/v, were prepared, keeping the concentration of 5% PVA_{3.5cP-98%} constant.

Scanning Electron Microscopy. The effects of (i) the cryoprotectant liquid and (ii) the combination of PVAs with different viscosities on the phantom microstructure were analyzed using SEM. Samples (each 1 cm thick) were cut from the PVA phantoms and kept overnight at −80 °C in a 50 mL conical tube (Falcon, Corning Inc., NY, US). The cap of the conical tube was removed and covered with parafilm. Tiny pores were created on the parafilm using a needle to ensure proper aeration and to allow water to evaporate from the sample. The sample was subsequently freeze-dried under vacuum at a temperature of −86 °C for 48 h to sublimate all the water content using a lyophilizer. Then, smaller cubic samples (approximately 1 mm thick on each side) were cut and sputter-coated with platinum for analysis. A field emission scanning electron microscope (JEOL, JSL 7600F, Tokyo, Japan) was used. The microstructure of each phantom sample was then visualized at 500× and 5000× magnification.

Density, Longitudinal Sound Speed, and Acoustic Attenuation Measurements. The density of the phantoms was measured based on the volume and mass of the phantoms,

which were determined by the water-displacement method¹⁵ and a precision weighing balance (SAB-220, Precision Electronic, Rachana Weigtech, Ahmedabad, Gujarat, India), respectively.

The longitudinal sound speed and acoustic attenuation were measured using the broadband pulse-echo, insertion-loss method.^{18,19} An ultrasound impulse was generated using a pulser-receiver (JSR DPR300, Imaginant, Rochester, USA) and sent to a single-element transducer (PA1415, Precision Acoustics Ltd., Dorchester, UK, active diameter: 10 mm, focal distance: 40 mm, bandwidth: 5–18 MHz), which served as both a transmitter and a receiver. A stainless-steel block, which served as an acoustic reflector, was positioned at the focus of the transducer in a degassed water tank. The reflected signal from the steel block without the phantom was recorded as the reference signal. Then, the phantom was inserted between the transducer and steel block to measure the acoustic attenuation through the phantom. The reflected signals were acquired using an oscilloscope (MD03014, Tektronix Inc., Bangalore, India; 100 MHz bandwidth, 2.5 Gs/s) and saved in a computer for postprocessing. Experiments were performed between water temperatures of 22–25 °C.

The longitudinal sound speed c_l in the phantom was calculated using the following formula:²⁰

$$c_l = \frac{c_w}{1 + \frac{c_w \Delta t}{2h}} \quad (1)$$

where c_w is the longitudinal sound speed in water, Δt is the time difference of an ultrasound signal in the presence and absence of the phantom, and h is the phantom thickness.

The frequency-dependent attenuation spectra of the phantoms $\alpha(f)$ were calculated as²⁰

$$\alpha(f) = 10 \log_{10} \left(\frac{|V_{\text{ref}}(f)|^2}{|V_{\text{phantom}}(f)|^2} \right) / 2h \quad (2)$$

where f is the frequency and V_{ref} and V_{phantom} are the amplitudes of the reflected ultrasound signals without and with the phantom, respectively. The attenuation coefficient (dB/cm) was calculated by power-law regression.¹⁵ Longitudinal sound speeds and attenuation coefficients were measured from five independent locations in each phantom sample and five independent samples per phantom type.

Ultrasound Elastography. Shear wave elastography was performed with a Vantage 128 system equipped with an L11–Sv linear array transducer (Verasonics, Kirkland, WA, USA). The center 32 elements of the array transducer were focused at a depth of 10 mm with a center frequency of 5.2 MHz to generate an acoustic radiation force impulse, resulting in shear wave propagation in the lateral direction, perpendicular to the axis of the transducer. The shear wave was then tracked at a high frame rate (10 kHz) by using plane wave imaging at a 7.6 MHz transmit frequency. The acquired in-phase/quadrature (IQ) data within a region of interest (8.6–11.5 mm axially within the −6 dB depth of focus²¹ and −10 to 10 mm laterally) was then processed to estimate the viscoelastic properties using a custom MATLAB script (R2019b, The MathWorks, Inc., Natick, MA, USA). The postprocessing steps for estimating the shear modulus and viscosity are outlined in Figure 1. A 2-D Loupas autocorrelator was used to calculate the axial displacement of the phantom.^{12,22} The sampling frequency of the data was subsequently increased by ten times using cubic-

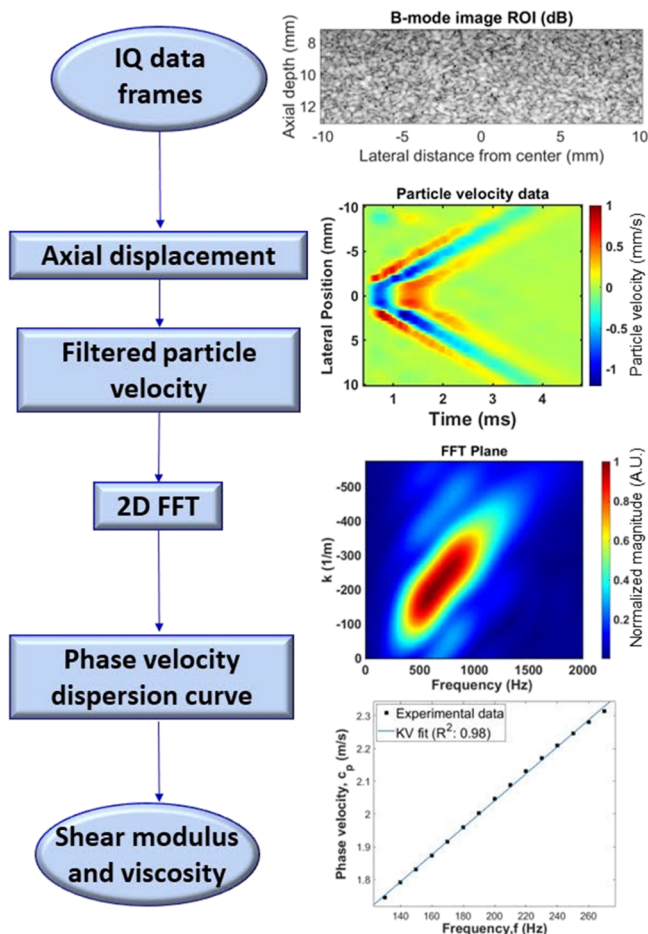


Figure 1. Flowchart of the postprocessing steps for shear modulus and viscosity estimation.

spline interpolation. The particle velocity was computed over time by using the finite-difference method. A Butterworth bandpass filter (10–800 Hz) and a median filter ($3\lambda \times 3\lambda$ kernel) were applied to smoothen the particle velocity data.^{12,23,24} Next, a 2D fast Fourier transform (FFT) of the shear wavefronts was performed, and the phase velocity (dispersion) curve was generated. To estimate the shear modulus and viscosity of each phantom, the phase velocity curve was fit to the Kelvin–Voigt (KV) model using least-squares nonlinear curve fitting based on the trust-region reflective algorithm.^{15,25,26} Assuming a homogeneous, isotropic medium and the planar nature of shear waves within the ROI, the phase velocity (c_s) based on the KV model is expressed as follows:²⁷

$$c_s(f) = \sqrt{\frac{2(G^2 + (2\pi f)^2 \eta^2)}{\rho(G + \sqrt{(G^2 + (2\pi f)^2 \eta^2)})}} \quad (3)$$

where G is the shear modulus, ρ is the density, f is the frequency, and η is the viscosity. Shear modulus and viscosity estimates were obtained for five independent imaging planes of each phantom sample and five samples of each phantom type.

Statistical Analyses. The mean and standard deviation (SD) of the density measurements were computed for five independent samples per phantom type. Power law regression was performed on the acoustic attenuation spectra to obtain the fit constant and exponent. The R^2 value was computed to

measure the goodness of fit. The mean and standard error of the mean of longitudinal sound speed, attenuation spectra, shear modulus, and viscosity measurements were calculated for five samples per phantom type. The Anderson–Darling test was performed to determine the normality of the data. For determining significant differences in density measurements, acoustic measurements, and viscoelasticity estimates, the *t* test, Wilcoxon rank sum test, analysis of variance (ANOVA), and Kruskal–Wallis tests were performed. For pairwise comparisons of data among different concentrations of PVA, Tukey's honest significant difference *post hoc* test was used. Statistical tests were performed at the 5% significance level using MATLAB and PRISM software (Version 9.5.1, GraphPad Inc., San Diego, CA, USA).

RESULTS

Effect of the Cryoprotectant Liquid on Density and Acoustic and Viscoelastic Properties of PVA Phantoms.

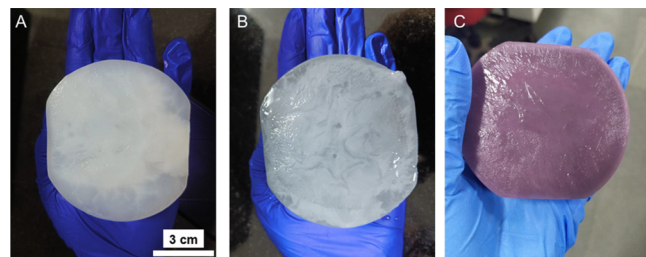


Figure 2. Photographs of phantoms with (A) only 8% (w/v) PVA, (B) 8% (w/v) PVA phantom with SiC particles, and (C) 8% (w/v) PVA with SiC particles and a 20% (w/v) cryoprotectant liquid. Scale bar = 3 cm.

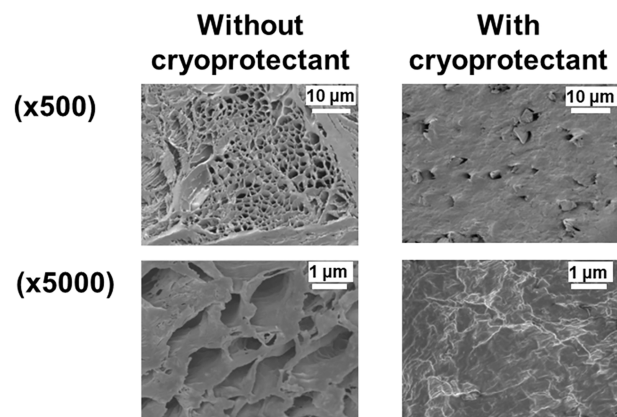


Figure 3. Representative SEM images of PVA phantoms without and with a cryoprotectant liquid at different magnifications.

Photographs of representative phantoms fabricated with and without a cryoprotectant liquid are shown in Figure 2. Inhomogeneous distributions of PVA within a phantom without and with SiC particles can be observed in Figure 2A,B, respectively. A phantom made with the cryoprotectant is shown in Figure 2C. The color of the cryoprotectant also resulted in a visually realistic “tissue-like” phantom.

Representative SEM images of phantoms with and without a cryoprotectant liquid are shown in Figure 3. The samples without a cryoprotectant had more porous structures than those with a cryoprotectant, which had smoother and homogenous microstructures.

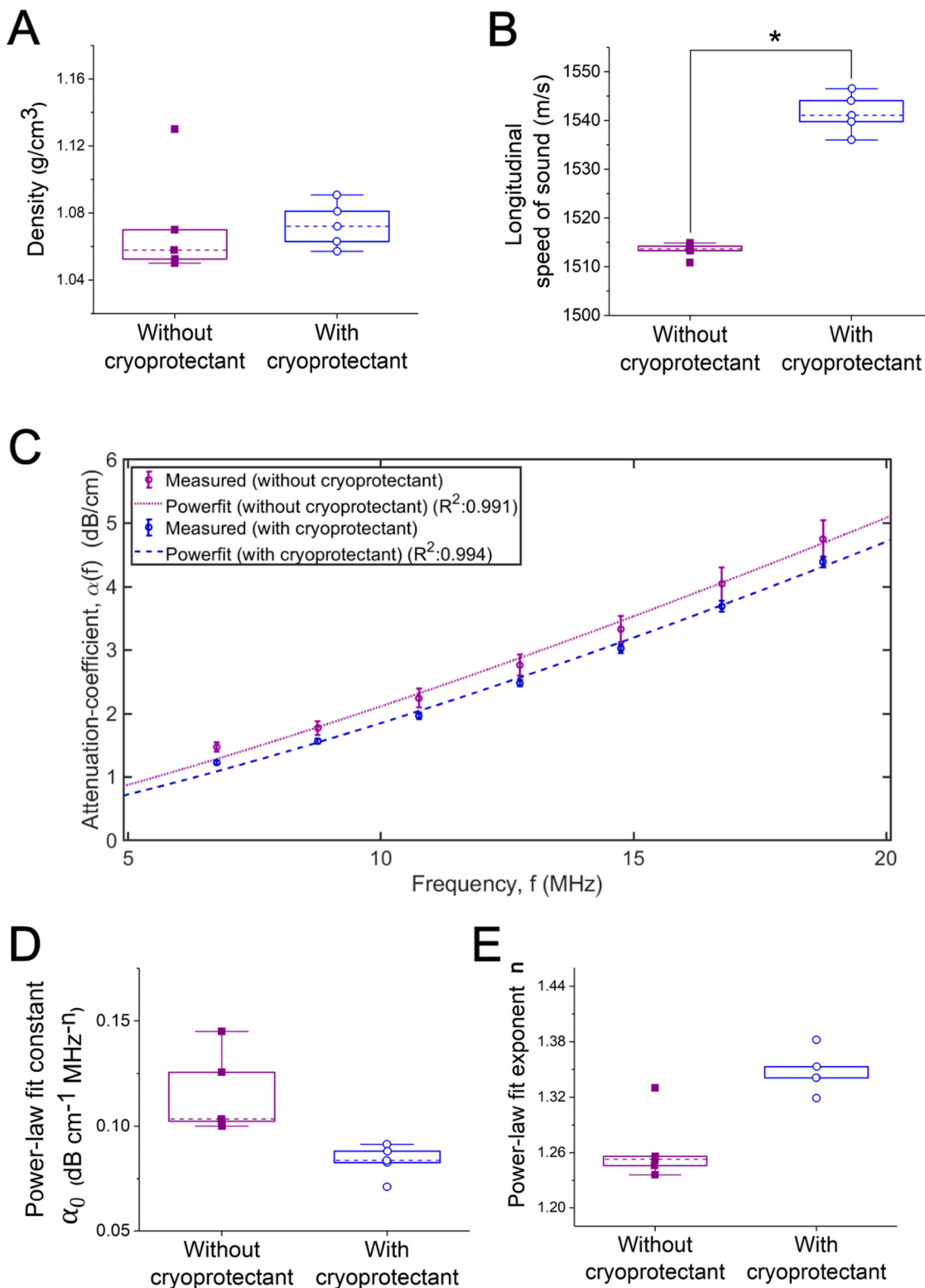


Figure 4. Box plots of (A) density and (B) longitudinal sound speed measurements. (C) Measured attenuation spectra of phantoms along with power-law fits. Mean \pm standard error of the mean from five independent phantoms are shown. Box plots of (D) the power-law fit constant α_0 and (E) the power-law fit exponent n derived from power-law regression of the attenuation spectra in (C). Individual data points are overlaid as closed squares (without a cryoprotectant) and open circles (with a cryoprotectant). * $p < 0.05$.

The density measurements of the phantoms are shown in Figure 4A. The data in the group without a cryoprotectant did not follow a normal distribution ($p = 0.02$). The rank sum test revealed that there was no significant difference between the

densities of phantoms with and without a cryoprotectant ($p = 0.42$).

The longitudinal sound speed measurements are shown in Figure 4B. The data were found to be normally distributed (p

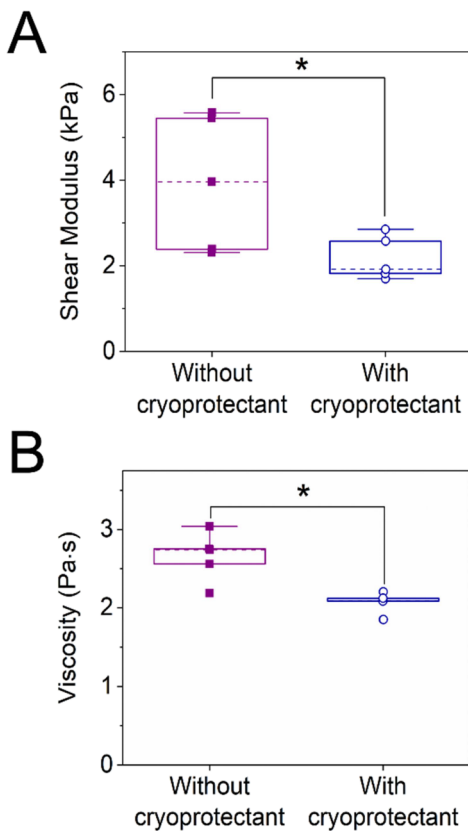


Figure 5. Box plots of (A) shear modulus and (B) viscosity measurements. Individual data points from five independent samples are overlaid as closed squares (without a cryoprotectant) and open circles (with a cryoprotectant). The dashed line represents the median values. * $p < 0.05$.

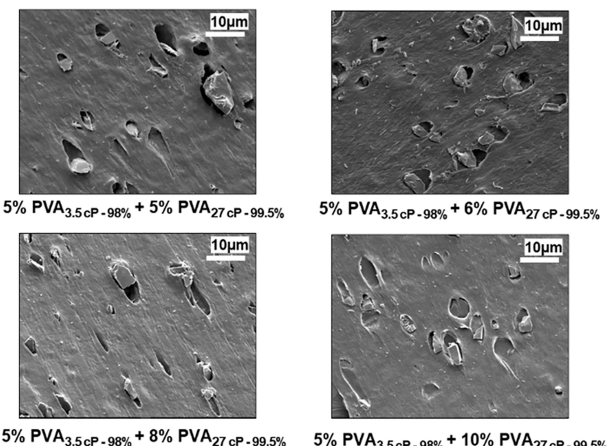


Figure 6. Representative SEM images of phantoms with different combinations of high- and low-viscosity PVA (500 \times magnification, scale bar = 10 μ m).

> 0.33). The longitudinal sound speeds were significantly different between phantoms without a cryoprotectant (1510–1514 m/s) and with a cryoprotectant (1536–1546 m/s) ($p < 0.001$).

The frequency-dependent attenuation spectra of the phantoms are shown in Figure 4C. The measured attenuation spectra over the 5–20 MHz bandwidth fit well with the power-law curve with R^2 values greater than 0.99 for all phantoms

with and without a cryoprotectant. The power-law fit constant (α_0) and exponent (n) are shown in Figure 4D,E, respectively.

Shear modulus and viscosity estimates of the phantoms are shown in Figure 5A,B, respectively. The shear modulus and viscosity data for all phantom compositions followed a normal distribution ($p > 0.25$ and $p > 0.13$, respectively). The viscoelasticity estimates for the phantoms without a cryoprotectant ($G = 3.93 \pm 0.7$ kPa; $\eta = 2.6 \pm 0.14$ Pa·s) were significantly different from those with a cryoprotectant ($G = 2.17 \pm 0.2$ kPa; $\eta = 2.0 \pm 0.05$ Pa·s) ($p = 0.03$ for shear modulus comparison and $p = 0.012$ for viscosity comparison). Moreover, the standard deviations in shear modulus and viscosity estimates were lower for phantoms with a cryoprotectant compared to those without cryoprotectant.

Effect of Combining PVA with Different Viscosities on the Density and Acoustic and Viscoelastic Properties of Phantoms. Representative SEM images of phantoms with 5% PVA_{3.5cP-98%} and four different concentrations of PVA_{27cP-99.5%} are shown in Figure 6. No noticeable differences were observed qualitatively in the microstructure of the phantoms.

The measured densities of the phantoms are shown in Figure 7A, which ranged from 1.021 to 1.357 g/cm³. The data from all groups followed a normal distribution ($p > 0.2$). One-way ANOVA revealed that there was no significant difference in the density of the phantoms ($p = 0.078$).

The longitudinal sound speed measurements of these phantoms are shown in Figure 7B, which ranged from 1540 to 1571 m/s. The data from all groups followed a normal distribution ($p > 0.07$). The Tukey's *post hoc* test revealed that the longitudinal sound speed measurements of compositions with 10% PVA_{27cP-99.5%} (1551–1571 m/s) were significantly different from the compositions with 5, 6, and 8% PVA_{27cP-99.5%} (1540–1554, 1542–1548, and 1549–1555 m/s), respectively ($p = 0.0034$, $p = 0.0005$, and $p = 0.03$, respectively).

The frequency-dependent attenuation spectra are shown in Figure 7C along with their corresponding power-law fit curves ($R^2 > 0.99$). Figure 7D,E includes the power-law fit constant and exponent, respectively, for the four types of phantoms fabricated.

The estimated shear moduli of phantoms with combinations of different concentrations of PVA_{3.5cP-98%} and PVA_{27cP-99.5%} are shown in Figure 8A. Shear modulus estimates increased with an increasing concentration of PVA_{27cP-99.5%} and varied from 3.3 to 17.7 kPa. The data points followed a normal distribution ($p > 0.13$ for all groups). All groups exhibited shear modulus values significantly different from each other ($p < 0.01$), except for 5% PVA_{27cP-99.5%} and 6% PVA_{27cP-99.5%} ($p = 0.08$).

The viscosity estimates are shown in Figure 8B, which varied from 2.6 to 7.3 Pa·s. Not all groups followed a normal distribution ($p = 0.020$ and 0.027 for 6 and 10% PVA_{27cP-99.5%}). Phantoms with 6% PVA_{27cP-99.5%} and 8% PVA_{27cP-99.5%} were not significantly different from each other ($p = 0.067$). Other phantom groups were significantly different from each other ($p < 0.001$).

DISCUSSION

The mechanical properties of PVA phantoms can vary based on the concentration of PVA in the phantom and the number of FT cycles while using one type of PVA, i.e., having a single viscosity or molecular weight. In this study, our focus was to develop and characterize phantoms with PVA of different

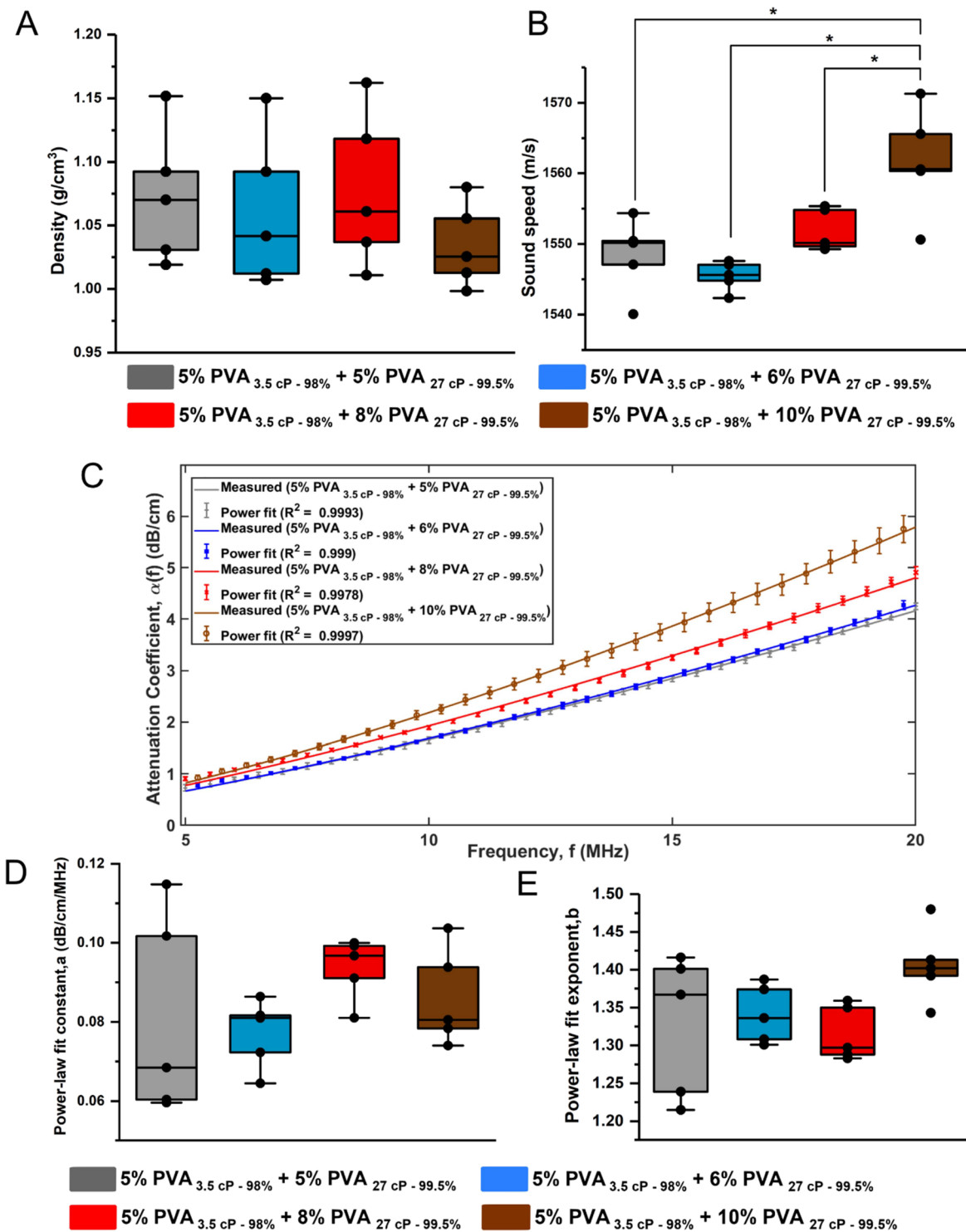


Figure 7. Box plots of (A) density and (B) longitudinal sound speed measurements of four phantom compositions. Individual data points are overlaid as closed circles ($n = 5$ samples). * $p < 0.05$. (C) Attenuation spectra measurements of phantoms from 5 to 20 MHz along with power-law fit curves. Mean \pm standard error of the mean is shown. Box plots of the power-law fit (D) constant and (E) exponent.

viscosities using a single FT cycle. We studied the effect of the cryoprotectant on the density and acoustic and viscoelastic properties of PVA phantoms.

The PVA phantoms with the cryoprotectant appeared to be more homogeneous (Figure 2) and were less porous (Figure 3) than those with PVA alone. Similar findings were observed in previous studies with PVA phantoms with glycerol, which exhibited nonporous structures.^{15,28} Similar to glycerol, the

cryoprotectant affects the cross-linking and gelation process.²⁹ The presence of a cryoprotectant in PVA phantoms helps in decreasing the freezing temperature and reducing the formation of tissue inhomogeneities.¹⁷

The measured density values of the fabricated phantoms (Figure 4A) were comparable to the density of soft tissues and previously reported values for PVA-based phantoms with and without a cryoprotectant.^{8,30} The longitudinal sound speed of

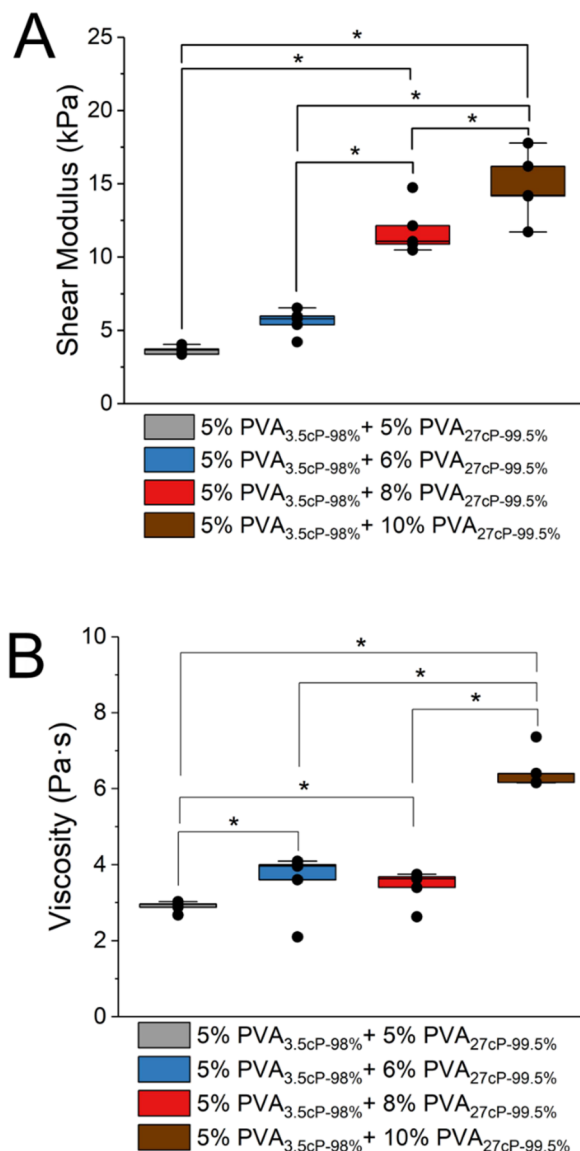


Figure 8. (A) Shear modulus and (B) viscosity measurements of phantoms with different compositions. Individual data points are overlaid as closed circles ($n = 5$ samples, $*p < 0.05$).

phantoms with the cryoprotectant closely approached the average speed in soft tissues (1540 m/s). Overall, the reported longitudinal sound speeds (Figure 4B) were consistent with those of soft tissues, such as breast and muscle.^{6,30,31} The attenuation measurements of phantoms fell within the range of soft tissue substitutes, such as gelatin, polyurethane, and PVA-based tissue-mimics,^{6,32} with power-law exponents comparable to those observed in soft tissues.³¹

The shear modulus estimates of phantoms (Figure 5A) were within the range of soft tissues.^{16,33,34} The phantoms with a cryoprotectant were significantly softer than those without a cryoprotectant (Figure 5A). Although prior studies that directly compare the moduli of PVA phantoms with and without a cryoprotectant do not exist, several studies have reported the moduli of PVA phantoms that contain a cryoprotectant. For example, Mercado-Shekhar et al. performed single-track location shear wave elastography of 8% w/v PVA phantoms with a 20% v/v cryoprotectant and found that the Young's modulus was 3.62 ± 0.07 kPa when subjected

to one freeze–thaw cycle.¹² Hansen et al. performed strain imaging on vascular phantoms containing 10 wt % PVA and found that the Young's modulus of the phantoms was 8.1 kPa after one freeze–thaw cycle.¹⁷ They also imaged phantoms with 15% PVA and found that the Young's modulus estimate increased to 98.8 kPa when subjected to two freeze–thaw cycles.

The viscosity estimates of phantoms with and without a cryoprotectant (Figure 5B) were also within the range of soft tissues.^{3,24,35} Chen et al. reported the viscosity of swine liver as 2.1 Pa·s using shear wave ultrasound vibrometry (SDUV) and the Voigt model fit to the dispersion curve.³⁶ Kumar et al. estimated the viscosity of breast using a Voigt model, which was in the range of 1–2 Pa·s.²⁴ Amador et al. measured the viscosity of the renal cortex in swine *in vitro* using SDUV to be 1.79 ± 0.38 Pa·s.³⁷ Notably, the variability in the shear modulus and viscosity estimates was less in phantoms with the cryoprotectant compared to those without the cryoprotectant, thereby indicating that the cryoprotectant leads to more homogeneous phantoms.

The compositions with partially hydrolyzed PVA, i.e., PVA_{2.5cP-80%} and PVA_{45cP-88%} (Table 1), could not form gel phantoms. This finding was contrary to Harpaz et al., who showed that partially hydrolyzed PVA (75–98%) is easily soluble in water.³⁸ PVA with lower degrees of hydrolysis has lower inter- and intramolecular H-bonds due to steric hindrance from acetate groups; hence, they interact more with water molecules.³⁸ The compositions with fully hydrolyzed PVA (greater than 98% hydrolysis), i.e., PVA_{3.5cP-98%} and PVA_{27cP-99.5%} phantoms, were able to form gel phantoms. The hydroxyl group in highly hydrolyzed PVA molecules form inter and intra H-bonds, thereby resulting in higher interaction with other PVA molecules and lower water solubility. Therefore, PVA with higher degrees of hydrolysis (>98%) dissolves at 50–100 °C.³⁹ In PVA with higher degrees of hydrolysis, decreasing the molecular weight increases solubility.³⁹ PVA's viscosity also has a significant impact on its water solubility, and thus, the gelation process.⁴⁰ The higher the viscosity of the solution, the greater the possibility of air bubble entrapment in the mixture during manufacturing.³¹ Interestingly, in the combination of two PVA grades, partially hydrolyzed PVA was not soluble entirely in the solution and resulted in formation of clumps. This result indicates a complex interplay among viscosity, molecular weight, and degree of hydrolysis from both PVA grades, affecting the subsequent gel formation.

Varying the concentration of PVA_{27cP-99.5%} while keeping PVA_{3.5cP-98%} constant did not result in any visible qualitative differences in the phantom microstructure (Figure 6). This observation may be attributed to the presence of the cryoprotectant, which could affect the phantom microstructure, similar to our observations in Figure 3.

The phantoms exhibited a range of viscoelastic properties by varying the concentration of PVA with different viscosities (Figure 8A,B). The shear modulus of the PVA phantoms increased with the increase in the concentration of PVA_{27cP-99.5%}, which has also been observed in previous studies.^{13,41} Noticeably, the relative differences in the mean viscosity estimates between 5%, 6%, and 8% PVA phantoms PVA_{27cP-99.5%} were lower (i.e., only at most 1.3 Pa·s difference) compared to those of the mean shear modulus estimates (i.e., up to 7.8 kPa difference). Thus, increasing the concentration of higher viscosity PVA while keeping the lower viscosity PVA constant resulted in small variations in viscosity estimates but

considerable differences in shear modulus. In contrast, Sharma et al. assessed PVA phantoms with different glycerol concentrations to modify its viscoelastic properties, but the viscosity estimates varied simultaneously with the shear modulus.¹⁵ The findings of our study are important as they can enable the preparation of phantoms with relatively constant viscosity and varying shear modulus.

LIMITATIONS AND FUTURE WORK

Although we showed the ability to fabricate viscoelastic tissue-mimicking PVA phantoms with a wide range of viscoelastic properties, further studies are needed to cover the entire spectrum of tissue characteristics. Freezing and thawing rates could potentially affect the viscoelastic parameters of the fabricated phantoms. Subsequent studies could investigate the effect of freezing and thawing rates on the acoustic and viscoelastic properties of PVA phantoms.

CONCLUSIONS

We reported an approach to tune the viscoelastic properties of PVA phantoms by mixing low- and high-viscosity PVA. In addition, we showed that adding a cryoprotectant to the phantom affected the viscoelastic properties and produced more homogeneous phantoms. The reported work can enable the preparation of homogeneous PVA phantoms with a broad viscoelasticity range for validating ultrasound elastography techniques.

AUTHOR INFORMATION

Corresponding Author

Karla P. Mercado Shekhar – Department of Biological Sciences and Engineering, Indian Institute of Technology Gandhinagar, Gandhinagar, Gujarat 382055, India; [ORCID iD](https://orcid.org/0000-0002-2533-5064); Email: [karlamshkhar@iitgn.ac.in](mailto:karlamshekhar@iitgn.ac.in)

Authors

Sapna R. Bisht – Department of Biological Sciences and Engineering, Indian Institute of Technology Gandhinagar, Gandhinagar, Gujarat 382055, India

Bhanu Prasad Marri – Department of Biological Sciences and Engineering, Indian Institute of Technology Gandhinagar, Gandhinagar, Gujarat 382055, India

Jayashree Karmakar – Department of Biological Sciences and Engineering, Indian Institute of Technology Gandhinagar, Gandhinagar, Gujarat 382055, India

Complete contact information is available at:
<https://pubs.acs.org/10.1021/acsomegab.3c09224>

Author Contributions

All authors have given approval to the final version of the manuscript. S.R.B. and B.P.M. contributed equally.

Funding

This work was supported by the Science and Engineering Research Board (Grant No. SRG/2021/001222), Government of India, and the Gujarat State Biotechnology Mission (Grant No. GSBTM/JD(R&D)/610/20–21/344).

Notes

The authors declare no competing financial interest.

ACKNOWLEDGMENTS

We thank Prof. Himanshu Shekhar and Dr. Nishita Mistry for their valuable feedback.

ABBREVIATIONS

PVA, poly(vinyl alcohol); SEM, scanning electron microscopy; FT, freeze–thaw; IQ_i, in-phase/quadrature; FFT, fast Fourier transform; KV, Kelvin–Voigt; SD, standard deviation; ANOVA, analysis of variance

REFERENCES

- (1) Rus, G.; Faris, I. H.; Torres, J.; Callejas, A.; Melchor, J. Why Are Viscosity and Nonlinearity Bound to Make an Impact in Clinical Elastographic Diagnosis? *Sensors* **2020**, *20* (8), 2379.
- (2) Lim, W. T. H.; Ooi, E. H.; Foo, J. J.; Ng, K. H.; Wong, J. H. D.; Leong, S. S. The Role of Shear Viscosity as a Biomarker for Improving Chronic Kidney Disease Detection Using Shear Wave Elastography: A Computational Study Using a Validated Finite Element Model. *Ultrasonics* **2023**, *133*, No. 107046.
- (3) Popa, A.; Bende, F.; Şirli, R.; Popescu, A.; Bâldea, V.; Lupaşoru, R.; Cotrău, R.; Fofiu, R.; Foncea, C.; Sporea, I. Quantification of Liver Fibrosis, Steatosis, and Viscosity Using Multiparametric Ultrasound in Patients with Non-Alcoholic Liver Disease: A “Real-Life” Cohort Study. *Diagnostics* **2021**, *11* (5), 783.
- (4) Dulgheriu, I. T.; Solomon, C.; Muntean, D. D.; Petea-Balea, R.; Lenghel, M.; Ciurea, A. I.; Dudea, S. M. Shear-Wave Elastography and Viscosity PLUS for the Assessment of Peripheric Muscles in Healthy Subjects: A Pre- and Post-Contraction Study. *Diagnostics* **2022**, *12*, 2138.
- (5) Palmeri, M. L.; Milkowski, A.; Barr, R.; Carson, P.; Couade, M.; Chen, J.; Chen, S.; Dhyani, M.; Ehman, R.; Garra, B.; Gee, A.; Guenette, G.; Hah, Z.; Lynch, T.; Macdonald, M.; Managuli, R.; Miette, V.; Nightingale, K. R.; Obuchowski, N.; Rouze, N. C.; Morris, D. C.; Fielding, S.; Deng, Y.; Chan, D.; Choudhury, K.; Yang, S.; Samir, A. E.; Shamdasani, V.; Urban, M.; Wear, K.; Xie, H.; Ozturk, A.; Qiang, B.; Song, P.; McAlaway, S.; Rosenzweig, S.; Wang, M.; Okamura, Y.; McLaughlin, G.; Chen, Y.; Napolitano, D.; Carlson, L.; Erpelding, T.; Hall, T. J. Radiological Society of North America/Quantitative Imaging Biomarker Alliance Shear Wave Speed Bias Quantification in Elastic and Viscoelastic Phantoms. *J. Ultrasound Med.* **2021**, *40* (3), 569–581.
- (6) Culjat, M. O.; Goldenberg, D.; Tewari, P.; Singh, R. S. A Review of Tissue Substitutes for Ultrasound Imaging. *Ultrasound Med. Biol.* **2010**, *36* (6), 861–873.
- (7) Cao, Y.; Li, G. Y.; Zhang, X.; Liu, Y. L. Tissue-Mimicking Materials for Elastography Phantoms: A Review. *Extrem. Mech. Lett.* **2017**, *17*, 62–70.
- (8) KMCGarry, C.; Grattan, L. J.; Ivory, A. M.; Leek, F.; Liney, G. P.; Liu, Y.; Miloro, P.; Rai, R.; Robinson, A. P.; Shih, A. J.; Zeqiri, B. Tissue Mimicking Materials for Imaging and Therapy Phantoms: A Review. *Phys. Med. Biol.* **2020**, *65*, 23T01.
- (9) Prokop, A. F.; Vaezy, S.; Noble, M. L.; Kaczkowski, P. J.; Martin, R. W.; Crum, L. A. Polyacrylamide Gel as an Acoustic Coupling Medium for Focused Ultrasound Therapy. *Ultrasound Med. Biol.* **2003**, *29* (9), 1351–1358.
- (10) Cafarelli, A.; Verbeni, A.; Poliziani, A.; Dario, P.; Menciassi, A.; Ricotti, L. Tuning Acoustic and Mechanical Properties of Materials for Ultrasound Phantoms and Smart Substrates for Cell Cultures. *Acta Biomater.* **2017**, *49*, 368–378.
- (11) Madsen, E. L.; A Hobson, M.; Shi, H.; Varghese, T.; R Frank, G. Tissue-Mimicking Agar/Gelatin Materials for Use in Heterogeneous Elastography Phantoms. *Phys. Med. Biol.* **2005**, *50*, 5597.
- (12) Mercado-Shekhar, K. P.; Kleven, R. T.; Aponte Rivera, H.; Lewis, R.; Karani, K. B.; Vos, H. J.; Abruzzo, T. A.; Haworth, K. J.; Holland, C. K. Effect of Clot Stiffness on Recombinant Tissue Plasminogen Activator Lytic Susceptibility in Vitro. *Ultrasound Med. Biol.* **2018**, *44* (12), 2710–2727.

- (13) Fromageau, J.; Brusseau, E.; Vray, D.; Gimenez, G.; Delachartre, P. Characterization of PVA Cryogel for Intravascular Ultrasound Elasticity Imaging. *IEEE Trans. Ultrason. Ferroelectr. Freq. Control* **2003**, *50* (10), 1318–1324.
- (14) Duboeuf, F.; Basarab, A.; Liebgott, H.; Brusseau, E.; Delachartre, P.; Vray, D. Investigation of PVA Cryogel Young's Modulus Stability with Time, Controlled by a Simple Reliable Technique. *Med. Phys.* **2009**, *36* (2), 656–661.
- (15) Sharma, A.; Marapureddy, S. G.; Paul, A.; Bisht, S. R.; Kakkar, M.; Thareja, P.; Mercado-Shekhar, K. P. Characterizing Viscoelastic Polyvinyl Alcohol Phantoms for Ultrasound Elastography. *Ultrasound Med. Biol.* **2022**, *49* (2), 497–511.
- (16) Cournane, S.; Fagan, A. J.; Browne, J. E. Review of Ultrasound Elastography Quality Control and Training Test Phantoms. *Ultrasound* **2012**, *20* (1), 16–23.
- (17) Hansen, H. H. G.; Saris, A. E. C. M.; Vaka, N. R.; Nillesen, M. M.; de Korte, C. L. Ultrafast Vascular Strain Compounding Using Plane Wave Transmission. *J. Biomech.* **2014**, *47* (4), 815–823.
- (18) Raymond, J. L.; Haworth, K. J.; Bader, K. B.; Radhakrishnan, K.; Griffin, J. K.; Huang, S. L.; McPherson, D. D.; Holland, C. K. Broadband Attenuation Measurements of Phospholipid-Shelled Ultrasound Contrast Agents. *Ultrasound Med. Biol.* **2014**, *40* (2), 410–421.
- (19) Shekhar, H.; Smith, N. J.; Raymond, J. L.; Holland, C. K. Effect of Temperature on the Size Distribution, Shell Properties, and Stability of Definity®. *Ultrasound Med. Biol.* **2018**, *44* (2), 434–446.
- (20) Selfridge, A. R. Approximate Material Properties in Isotropic Materials. *IEEE Trans. Sonics Ultrasonic* **1985**, *32*, 381–384, DOI: 10.1109/T-SU.1985.31608.
- (21) Palmeri, M. L.; Wang, M. H.; Dahl, J. J.; Frinkley, K. D.; Nightingale, K. R. Quantifying Hepatic Shear Modulus In Vivo Using Acoustic Radiation Force. *Ultrasound Med. Biol.* **2008**, *34* (4), 546–558.
- (22) Loupas, T.; Powers, J. T.; Gill, R. W. An Axial Velocity Estimator for Ultrasound Blood Flow Imaging, Based on a Full Evaluation of the Doppler Equation by Means of a Two-Dimensional Autocorrelation Approach. *IEEE Trans. Ultrason. Ferroelectr. Freq. Control* **1995**, *42* (4), 672 DOI: 10.1109/58.393110.
- (23) Hollender, P. J.; Rosenzweig, S. J.; Nightingale, K. R.; Trahey, G. E. Single- and Multiple-Track-Location Shear Wave and Acoustic Radiation Force Impulse Imaging: Matched Comparison of Contrast, Contrast-to-Noise Ratio and Resolution. *Ultrasound Med. Biol.* **2015**, *41* (4), 1043–1057.
- (24) Kumar, V.; Denis, M.; Gregory, A.; Bayat, M.; Mehrmohammadi, M.; Fazzio, R.; Fatemi, M.; Alizadid, A.; Kumar, V.; Denis, M.; Gregory, A.; Bayat, M.; Mehrmohammadi, M.; Fazzio, R.; Fatemi, M.; Alizad, A. Viscoelastic Parameters as Discriminators of Breast Masses: Initial Human Study Results. *PLoS One* **2018**, *13* (10), No. e0205717.
- (25) Poul, S. S.; Ormachea, J.; Ge, G. R.; Parker, K. J. Comprehensive Experimental Assessments of Rheological Models' Performance in Elastography of Soft Tissues. *Acta Biomater.* **2022**, *146*, 259–273.
- (26) Parker, K. J.; Szabo, T.; Holm, S. Towards a Consensus on Rheological Models for Elastography in Soft Tissues. *Phys. Med. Biol.* **2019**, *64*, 215012 DOI: 10.1088/1361-6560/ab453d.
- (27) Poul, S. S.; Parker, K. J. Fat and Fibrosis as Confounding Cofactors in Viscoelastic Measurements of the Liver. *Phys. Med. Biol.* **2022**, *66* (4), No. 045024.
- (28) Wang, T.; Chen, L.; Shen, T.; Wu, D. Preparation and Properties of a Novel Thermo-Sensitive Hydrogel Based on Chitosan/Hydroxypropyl Methylcellulose/Glycerol. *Int. J. Biol. Macromol.* **2016**, *93*, 775–782.
- (29) Cournane, S.; Cannon, L.; Browne, J. E.; Fagan, A. J. Assessment of the Accuracy of an Ultrasound Elastography Liver Scanning System Using a PVA-Cryogel Phantom with Optimal Acoustic and Mechanical Properties. *Phys. Med. Biol.* **2010**, *55* (19), 5965–5983.
- (30) Zell, K.; Sperl, J. I.; Vogel, M. W.; Niessner, R.; Haisch, C. Acoustical Properties of Selected Tissue Phantom Materials for Ultrasound Imaging. *Phys. Med. Biol.* **2007**, *52*, N475.
- (31) Braunstein, L.; Brüningk, S. C.; Rivens, I.; Civale, J.; Ter Haar, G. Characterization of Acoustic, Cavitation, and Thermal Properties of Poly(Vinyl Alcohol) Hydrogels for Use as Therapeutic Ultrasound Tissue Mimics. *Ultrasound Med. Biol.* **2022**, *48* (6), 1095–1109.
- (32) Surry, K. J. M.; Austin, H. J. B.; Fenster, A.; Peters, T. M. Poly(Vinyl Alcohol) Cryogel Phantoms for Use in Ultrasound and MR Imaging. *Phys. Med. Biol.* **2004**, *49* (24), 5529–5546.
- (33) Hoskins, P. R. Principles of Ultrasound Elastography. *Ultrasound* **2012**, *20* (1), 8–15.
- (34) Bots, M. L.; Evans, G. W.; Riley, W. A.; Grobbee, D. E. Carotid Intima-Media Thickness Measurements in Intervention Studies. *Stroke* **2003**, *34* (12), 2985–2994.
- (35) Petea-Balea, D. R.; Solomon, C.; Muntean, D. D.; Dulgheriu, I. T.; Silaghi, C. A.; Dudea, S. M. Viscosity Plane-Wave UltraSound (Vi PLUS) in the Evaluation of Thyroid Gland in Healthy Volunteers—A Preliminary Study. *Diagnostics* **2022**, *12* (10), 2474.
- (36) Chen, S.; Urban, M. W.; Pislaru, C.; Kinnick, R.; Zheng, Y.; Yao, A.; Greenleaf, J. F. Shearwave Dispersion Ultrasound Vibrometry (SDUV) for Measuring Tissue Elasticity and Viscosity. *IEEE Trans. Ultrason. Ferroelectr. Freq. Control* **2009**, *56* (1), 55.
- (37) Amador, C.; Urban, M. W.; Greenleaf, J. F.; Warner, L. V. Measurements of Swine Renal Cortex Shear Elasticity and Viscosity with Shearwave Dispersion Ultrasound Vibrometry (SDUV). In *IEEE International Ultrasonics Symposium*; IEEE, 2009; pp. 491–494.
- (38) Harpaz, D.; Axelrod, T.; Yitian, A. L.; Eltzov, E.; Marks, R. S.; Tok, A. I. Y. Dissolvable Polyvinyl-Alcohol Film, a Time-Barrier to Modulate Sample Flow in a 3D-Printed Holder for Capillary Flow Paper Diagnostics. *Materials* **2019**, *12* (3), 343.
- (39) Chan, L. W.; Hao, J. S.; Heng, P. W. S. Evaluation of Permeability and Mechanical Properties of Composite Polyvinyl Alcohol Films. *Chem. Pharm. Bull.* **1999**, *47* (10), 1412–1416.
- (40) Xue, R.; Xin, X.; Wang, L.; Shen, J.; Ji, F.; Li, W.; Jia, C.; Xu, G. A Systematic Study of the Effect of Molecular Weights of Polyvinyl Alcohol on Polyvinyl Alcohol–Graphene Oxide Composite Hydrogels. *Phys. Chem. Chem. Phys.* **2015**, *17* (7), 5431–5440.
- (41) Sharifi, F.; Bai, Z.; Montazami, R.; Hashemi, N. Mechanical and Physical Properties of Poly (Vinyl Alcohol) Microfibers Fabricated by a Microfluidic Approach. *RSC Adv.* **2016**, *6*, 55343–55353.